Citation
He, S. and Chen, K. and Saunders, M. and Quadir, Z. and Tao, S. and Irvine, J. and Cui, C. et al. 2018. Interface formation and Mn segregation of directly assembled La0.8Sr0.2MnO3 cathode on Y2O3-ZrO2 and Gd2O3-CeO2 electrolytes of solid oxide fuel cells. Solid State Ionics. 325: pp. 176-188
http://doi.org/10.1016/j.ssi.2018.08.016

Interface Formation and Mn Segregation of Directly Assembled $La_{0.8}Sr_{0.2}MnO_3$ Cathode on Y_2O_3-ZrO_2 and Gd_2O_3-CeO_2 Electrolytes of Solid Oxide Fuel Cells

Shuai He,[a,b] Kongfa Chen,[c] Martin Saunders,[d] Zakaria Quadir,[e] Shanwen Tao,[f] John T.S. Irvine,[g] C. Q. Cui,[a,*] and San Ping Jiang[a,b,h*]

[a]School of Electromechanical Engineering, Guangdong University of Technology, Guangzhou 51006, People's Republic of China

[b] Fuels and Energy Technology Institute & Western Australian School of Mines: Minerals, Energy and Chemical Engineering, Curtin University, Perth, WA 6102, Australia

[c] College of Materials Science and Engineering, Fuzhou University, Fuzhou 350108, China

[d] Centre for Microscopy, Characterisation and Analysis, The University of Western Australia, Perth, WA 6009, Australia

[e] Microscopy and Microanalysis Facility, John de Laeter Centre, Curtin University, Perth, WA 6102, Australia

[f] Department of Chemical Engineering, Monash University, Clayton, Victoria 3800, Australia

[g] School of Chemistry, University of St Andrews, Fife KY16 9ST, UK

[h] Faculty of Science, Health, Education and Engineering, University of Sunshine Coast, Maroochydore DC, Queensland 4558, Australia

Corresponding Author: cqcui01@qq.com (CQ Cui); s.jiang@curtin.edu.au (SP Jiang)

Abstract:

The establishment of intimate electrode/electrolyte interface is very important in solid oxide fuel cells (SOFCs), because it plays a critical role in the overall cell performance and durability. In this study, Mn segregation and interface formation between directly assembled $La_{0.8}Sr_{0.2}MnO_3$ (LSM) electrode and yttrium-stabilized zirconia (YSZ) or gadolinium-doped

ceria (GDC) electrolytes are studied using combined focused ion beam and scanning transmission electron microscopy (FIB-STEM). In the case of LSM/YSZ and LSM/GDC electrodes, a significant reduction in the electrode ohmic resistance is observed after cathodic polarization at 900ºC and 500 $mAcm^{-2}$, indicating the formation of an intimate interface. However, LSM particles start to disintegrate at the electrode/electrolyte interface with the increase of polarization time in the case of LSM/YSZ electrode. On the other hand, the LSM/GDC interface is very stable with negligible microstructure change at the interface. Mn segregation from the LSM perovskite structure is identified under the influence of polarization in both LSM/YSZ and LSM/GDC electrodes. The results demonstrate that nature of the electrolyte plays a critical role in the electrochemical activity, microstructure, morphology and stability of LSM/electrolyte interface under SOFC operation conditions.

Keywords: solid oxide fuel cells; direct assembly; LSM cathodes; YSZ and GDC electrolyte; interface; Mn segregation.

1. Introduction

Solid oxide fuel cells (SOFCs) are energy conversion devices to efficiently produce electricity from chemical energy of a wide variety of fuels, such as hydrogen, natural gas and hydrocarbons[1-5]. SOFCs are considered as environmentally friendly technologies with significantly less greenhouse gas emission as compared to the coal combustion plants[6, 7]. Typical SOFC cells consist of Ni-yttria-stabilized zirconia (Ni-YSZ) cermet anodes, YSZ electrolyte and lanthanum strontium manganite (LSM) perovskite cathode. Generally, the ceramic components of the SOFC devices are pre-sintered at high temperatures, e.g., ~1400ºC for Ni-YSZ cermet anode and ~1150ºC for LSM cathodes[8-10] to establish an intimate electrode/electrolyte interface. The performance of SOFCs not only depends on the

electrocatalytic activity of electrode materials, but also the microstructure of the electrode/electrolyte interface[11-14].

LSM perovskite is one of the most commonly and widely investigated cathode materials due to its high electronic conductivity and excellent electrocatalytic activity for oxygen reduction reaction (ORR) at high temperatures[10, 15, 16]. As LSM is predominantly an electronic conductor with negligible ionic conductivity, the ORR mainly occur at the triple phase boundary (TPB) where the oxygen, electrode and electrolyte meet. The formation of an intimate electrode/electrolyte interface is thus critical in determining the performance and durability of SOFC cells. This is because the interface provides a direct pathway for oxygen species migration from electrode to electrolyte. In the case of LSM cathode pre-sintered at high temperatures, the interface is characterized by the formation of convex contact rings on YSZ and GDC electrolyte surface[14, 17-22]. On the other hand, it has been known that cathodic polarization has a significant effect on the electrode/electrolyte interface under the fuel cell operation conditions. This is reflected from the formation of micro-pores and dense layers at the interface[19, 23-25], the increase in TPB length[26] and the change in electrolyte morphology[21, 27]. Early studies show that polarization can broaden and flatten the edges of the contact rings[18]. The distinct topography change of the convex contact rings is most likely due to the incorporation of oxygen and/or interdiffusion between LSM and YSZ electrolyte at the interface. The microstructural change at the electrode/electrolyte interface during long-term cathodic polarization can also lead to a significant cell performance degradation. Appel et al.[24] reported that after polarization at 300 $mAcm^{-2}$ and 1000 ^{o}C for 2000 h, the overpotential of a LSM-YSZ composite cathode based cell exceeds by 100% of the initial value. The morphology changes at the interface due to pore formation and densification of the electrode layer were considered as the main reasons for the increase in the polarization resistance during the stability test.

Recently, we have shown the feasibility of applying directly assembled electrode on electrolyte without requiring further high temperature sintering, and the *in situ* formation of electrode/electrolyte interface induced by cathodic polarization[28-37]. In the case of LSM electrode and YSZ electrolyte (LSM/YSZ), the results indicate that the electrochemical performance of the cathodic polarization induced interface is comparable to that of the conventional pre-sintered electrodes, though the topography of the interface is very different, i.e. the formation of convex contact rings for the thermally induced interface and contact clusters for the electrochemically induced interface[28]. The formation of the electrochemically induced LSM/YSZ interface is accompanied by the pronounced decrease of electrode ohmic resistance, particularly at the initial stage of polarization[31]. Studies show that LSM is thermally compatible with YSZ and GDC electrolytes and the formation of lanthanum zirconate only occurs at a higher temperature of 1300 ^{o}C in the case of LSM/YSZ but in the case of LSM/GDC, no interfacial reaction was observed [22]. However, the evolution of the electrode/electrolyte interface under the influence of cathodic polarization as well as the fundamental understanding of the crystallographic and compositional changes of the polarization induced interface in the case of directly assembled LSM electrodes are still unclear at this stage.

In this paper, a comparative study was carried out on the electrochemical activity, interface formation and Mn segregation of the directly assembled LSM electrode on YSZ or GDC electrolytes using combined FIB-STEM technique. The results indicate that the electrochemical performance of directly assembled LSM/YSZ and LSM/GDC electrodes is greatly enhanced by the cathodic polarization. The electrode/electrolyte hetero-interface formed under cathodic polarization is characterized by the periodic lattice plane matching, accompanied by the presence of lattice mismatch and distortion. The nature of the electrolyte

shows a significant effect on the stability of the interface formed between LSM and YSZ or GDC electrolyte.

2. Experimental

2.1. Fabrication of direct assembled LSM electrode on YSZ or GDC electrolyte

$La_{0.8}Sr_{0.2}MnO_3$ (LSM) cathode powder was synthesized via sol-gel method, using $La(NO_3)_3 \cdot 6H_2O$ (99.9%, A.R., Alfa Aesar, UK), $Sr(NO_3)_2$ (99%, A.R., Sigma-Aldrich, US), $Mn(NO_3)_2$ (50 wt% solution, A.R., Alfa Aesar, UK) as raw materials, and anhydrous citric acid (99.5%, A.R., Chem Supply, Australia), ethylenediaminetetraacetic acid (EDTA, 99%, Acros Organics, Australia) and ammonia solution (28%w.w., Sigma-Aldrich, US) as complexing agents with a molar ratio of 1:1.5:1 (metal ions/citric acid/EDTA). Stoichiometric metal nitrates were blended with deionized water, and the calculated amounts of citric acid, EDTA and ammonia solution were subsequently added. The pH of the solution was adjusted to 7 and the solution was stirred on a hot plate until the dry gel was formed. The resultant gel powder was calcined at 1000°C for 2 h.

Electrolyte pellets were fabricated by die-pressing powders of 8 mol% Y_2O_3 doped ZrO_2 (YSZ, Tosoh, Japan) and $Gd_{0.1}Ce_{0.9}O_{1.95}$ (GDC, AGC Seimi Chemical Co Ltd), followed by sintering at 1450°C for 5 h. The pellets were approximately 1 mm in thickness and 18 mm in diameter. Pt paste (Gwent Electronic Materials Ltd., UK) was painted on the centre and ring of the electrolyte, and sintered at 1100°C for 2 h as the counter and reference electrodes. LSM powder was thoroughly mixed with an ink vehicle (Fuel Cell Materials, US) at a weight ratio of 5:5 in an agate mortar to form a uniform electrode paste. The paste was subsequently screen-printed on the other side of the electrolyte pellet symmetrically opposite to the Pt counter electrode and then dried at 100°C for 2h to form the directly assembled cathode/electrolyte electrodes without further high temperature pre-sintering step [38].

2.2. Characterization

Electrochemical performance of directly assembled LSM/YSZ and LSM/GDC electrodes was measured using a Zahner Electrochemical Workstation. The electrodes were cathodically polarized at 750 ^{o}C and 500 mAcm^{-2} for 1 or 12 h, and electrochemical impedance was measured under open circuit conditions in a frequency range of 0.1 Hz to 100 kHz with a signal amplitude of 20 mV. Air was supplied to the cathode side at a flow rate of 100 mL min^{-1}. Electrode ohmic resistance (R_{Ω}) was obtained from the high frequency intercept, and electrode polarization resistance (R_{p}) was obtained from the differences between the low- and high-frequency intercepts of the impedance curves.

The microstructure of the electrolyte surface in contact with LSM was examined by scanning electron microscopy (SEM, Zeiss Neon 40EsB, Germany). In order to examine the morphology of the electrolyte surface, the LSM coating was completely removed by HCl (32 wt%, Sigma-Aldrich, US) treatment, and in some cases, the electrode was partly peeled off to study the electrode/electrolyte interface. The topographic features of the acid cleaned electrolyte surface were examined by atomic force microscopy (AFM, Alpha 300 SAR, WITec GmbH, Ulm Germany) at intermittent contact mode. Electrolyte lamella in contact with LSM particle was lifted out and milled to around 70 nm in thickness using FEI Helios Nanolab G3 CX Dual Beam Focused Ion Beam - Scanning Electron Microscope (FIB-SEM, Helios Nanolab G3 CX, FEI company, US) with Ga^{+} ion source. The elemental mapping and microstructural micrographs were obtained on the FIB milled sample using a high angle annular dark field scanning transmission electron microscopy (HAADF-STEM, FEI Titan G2 80-200 TEM/STEM with ChemiSTEM Technology, US) at 200 kV. The fast Fourier transform (FFT) images were extracted using TEM Imaging & Analysis software (TIA, FEI Company, US) to examine the diffraction behavior of selected areas, and inverse FFT (IFFT) simulations were

performed on Gatan Digital Micrograph (Gatan Digital Microscopy Suite, Gatan Inc., US) to reconstruct the selected lattice planes using FFT images.

3. Results and Discussion

3.1 Electrochemical performance of directly assembled LSM/YSZ and LSM/GDC electrodes

Fig. 1 shows the electrochemical performance of the directly assembled LSM cathode on YSZ and GDC electrolytes after polarization at 900 ^{o}C and 500 mAcm^{-2} for 12 h. The electrochemical activity of the LSM/YSZ electrode for ORR improves significantly with the cathodic polarization. R_p was remarkably reduced from 60.0 Ω cm^2 to 0.8 Ω cm^2 and R_Ω decreased from 2.1 Ω cm^2 to 0.9 Ω cm^2 after polarization (Fig.1a). The cathode potential measured between LSM electrode and Pt reference electrode ($E_{cathode}$) also dropped quickly from its initial value of 1.3 V to ~0.9 V under the influence of cathodic polarization. For the LSM/GDC electrode, the electrochemical performance also experiences a significant improvement (see Fig. 1b). The initial R_Ω and R_p were 1.1 Ω cm^2 and 1.0 Ω cm^2, respectively, and decreased to 0.6 Ω cm^2 and 0.3 Ω cm^2 after polarization for 12 h. The $E_{cathode}$ also decreases gradually from 0.55V to 0.45V. The significantly enhanced activity is due to the well-known activation behaviour of LSM-based cathode [10, 14, 39-44]. The significant decrease in the R_Ω for both LSM/YSZ and LSM/GDC electrodes implies the establishment of cathode/electrolyte interface under the influence of cathodic polarization, as in the case of pre-sintered LSM/YSZ and LSM/GDC electrodes, there is no change in R_Ω under similar cathodic polarization conditions [22, 31]. It is noted that R_p for ORR on LSM/GDC electrode is significantly smaller than that on LSM/YSZ electrode under identical conditions (e.g., 1.0 Ω cm^2 *vs* 60.0 Ω cm^2 at the initial polarization stage), indicating that the high ionic conductivity of GDC electrolyte promotes the ORR on LSM electrode. This is consistent with the observed strong dependence of the electrocatalytic activity of mixed ionic and electronic conducting cathodes for ORR on the properties of the electrolyte, as shown by Liu and Wu[45] and by Philippeau et al[46].

3.2 Microstructure of the polarization induced interface

The microstructure of the YSZ and GDC electrolytes surface in contact with LSM cathode before and after polarization is presented in Fig. 2 and Fig. 3, respectively. For the LSM/YSZ electrode, the morphology of the electrolyte surface was greatly changed after polarization at 900 ^{o}C and 500 mAcm^{-2} for just 1 h (Fig.2). Pure YSZ electrolyte surface without contact with LSM coating was smooth and flat and grain size of YSZ was 3.77 ± 3.12 μm (Fig. 2e). The formation of ring-shaped contact marks was observed and the diameter of the contact marks was in the range of 0.57-1.1 μm (Fig. 2b). The dimension of the ring-shaped contact marks is close to that of the LSM particles of the directly assembled LSM, 1.27 ± 0.54 μm (Fig.2a). Within the contact rings, a considerable number of particles with a dimension of 28.8 ± 8.4 nm were found, indicating the possible disintegration of the LSM particles under the influence of polarization. After the polarization for 12 h, the ring-shaped contact marks continue to grow and merge together, forming contact craters with dimension as large as 2 μm on the YSZ electrolyte (Fig. 2c and d). Matsui *et al*. also observed the significant microstructural change at the interface between pre-sintered LSM electrode and YSZ electrolyte and the increase of roughness of YSZ surface both in and out of contact with LSM particles with the increase of the polarization time at 1000 ^{o}C [14]. An increase in the length of three phase boundary was observed after polarization at 200 mA cm^{-2} for 5 h.

In the case of LSM/GDC electrode, the change in the morphology of GDC electrolyte is much smaller during the cathodic polarization as compared to that on YSZ electrolyte (see Fig. 3). For instance, after polarization for 1 h, the morphology of the GDC electrolyte surface was still smooth with a formation of small and shallow ring-shaped contact marks, as shown in Fig. 3a and b. After polarization for 12 h, the contact marks also grew in size (Fig. 3d), but no ring-shaped contact marks were found as in the case of LSM/YSZ electrode (Fig.2d). The changes in the microstructure of GDC electrolyte in contact with LSM under the influence of

polarization are much less significant as compared to that of YSZ electrolyte. The morphology of pristine GDC electrolyte surface is also smooth with distribution of large and small GDC grains (Fig.3e). The average grain size was 1.19 ± 1.04 μm.

Fig. 4 shows the AFM topography of the YSZ and GDC electrolyte surfaces in contact with LSM cathode. LSM electrodes were removed by acid treatment. In the case of LSM/YSZ electrode, convex contact rings with a dimension of 1.14 ± 0.54 μm was formed on the YSZ surface after the cathodic polarization for 1 h (Fig. 4a). After polarization for 12 h, the contact rings grew significantly, and the dimension of the rings increased to 1.80±0.71 μm (Fig.4b). The AFM line scan across the edge of the contact rings revealed the ring depth profile of 0.14±0.06 μm (Fig.4c), showing the significant roughening of the YSZ electrolyte surface. For the LSM/GDC electrode, the change in the electrolyte morphology is almost negligible after polarization for 1 h (Fig. 4d). After polarization for 12 h, the formation of contact clusters or marks on GDC electrolyte surface became clearly visible (Fig.4e). The average dimension of these clusters was 0.22±0.09 μm with the depth profile of 5.2±0.7 nm (Fig.4f), substantially smaller than that on YSZ electrolyte. The relatively small microstructure change of the GDC electrolyte at the interface implies that the LSM cathode is more stable with GDC as compared to that with YSZ under the influence of polarization, consistent with the thermal compatibility studies[22].

Fig. 5 presents the LSM/YSZ and LSM/GDC interface lamella prepared by FIB, taking in the interface regions as shown in Figs. 2 and 3. The TEM images of the electrode/electrolyte interfaces clearly demonstrate the interface evolution under the influence of cathodic polarization. For example, in the case of LSM/YSZ electrode, it appears that the LSM particle started to disintegrate at the electrode/electrolyte interface after the polarization for 1 h, forming discrete contact areas with the electrolyte. With further polarization for 12 h, the

disintegration of the LSM cathode particle at the interface became clearly visible (Fig. 5b). In the case of LSM/GDC electrode, no visible disintegration of the LSM cathode particle was observed. After polarization for 1 h, an intimate and void-free contact between LSM and GDC electrolyte was established (Fig. 5c). The interface appears stable after polarization for 12 h (Fig.5d), very different to the LSM/YSZ interface.

3.4 LSM/YSZ interface

Fig. 6 shows the STEM-EDS and HRTEM results of a directly assembled LSM cathode on YSZ electrolyte after polarization at 900 ^{o}C and 500 mAcm^{-2} for 1 h. There was a disintegration at the interface and a clear presence of La, Sr and Mn was observed in the disintegrated nanoparticles (Fig.6a). A strong accumulation of Mn was also observed on the surface of one of the LSM particles, indicating the Mn segregation under the influence of cathodic polarization. Nevertheless, the segregated Mn was not observed at the electrode/electrolyte interface, indicating that segregated Mn species from LSM perovskite structure may not migrate to the interface under the cathodic polarization conditions. The HRTEM analysis shows an intimate contact between the LSM particle and YSZ electrolyte with lattice planes meeting and matching at the interface. For example, the particle can be identified by the periodic lattice arrangement of $\{202\}_{\mathrm{LSM}}$ planes with a plane spacing of 0.22 nm[47, 48], indicating that disintegrated particles exist as LSM perovskite phase. The YSZ electrolyte is characterized by the $\{111\}_{\mathrm{YSZ}}$ lattice planes with plane spacing of 0.29 nm[49]. In this instance the orientation relationship, *i.e.*, the angle between the $\{202\}_{\mathrm{LSM}}$ and $\{111\}_{\mathrm{YSZ}}$ lattice planes at the interface, was found to be $\theta_{\{202\}\mathrm{LSM}/\{111\}\mathrm{YSZ}} = 46.9^{o}$, and the mismatch factor (*f*) [50-53] for these two planes can also be calculated:

$$f = \frac{d_{\{111\}YSZ} - d_{\{202\}LSM}}{d_{\{111\}YSZ}} * 100\% = 24.1\% \qquad [1]$$

However, it should be noted that the current examined interface and the orientation relationship between $\{202\}_{LSM}$ and $\{111\}_{YSZ}$ lattice planes may be different at different locations, as a result of the polycrystalline nature of both phases. The establishment of the interface between disintegrated LSM particles and YSZ electrolyte is supported by the significant decrease in R_Ω.

The disintegration of LSM cathode particle at the electrode/electrolyte interface is significant after polarization at 900°C and 500 $mAcm^{-2}$ for 12 h, as shown in Fig. 7. The portion of the LSM particle in contact with YSZ electrolyte decomposed into a large number of small particles with the formation of voids in the bulk, and Mn segregation was also observed. In the disintegrated LSM particles, there is a presence of Zr and Y in addition to La, Sr and Mn, implying the interaction and formation of La-Mn-Zr solid solution[54-57]. Although the formation of $La_2Zr_2O_7$ cannot be ruled out at this stage, the continuous decrease of R_Ω during the polarization may indicate that the presence of such solid solutions between LSM and YSZ on the ORR is negligible and insignificant[58]. The atomic geometry of the hetero-interface between the YSZ electrolyte and the disintegrated LSM particles shows the lattice plane matching of the LSM and YSZ phases at the interface, *i.e.*, YSZ phase with $\{220\}_{YSZ}$ planes and plane spacing of 0.18 nm and LSM with $\{202\}_{LSM}$ planes and plane spacing of 0.22 nm (Fig. 7b). The orientation relationship between the two examined planes was found to be $\theta_{\{202\}LSM/\{220\}YSZ} = 50.0^o$ with a lattice mismatch factor of f=18.2%. The FFT diffractogram of the electrolyte shows a typical cubic YSZ structure[49, 59], while for the LSM phase, it appears to be an overlap of two sets of same patterns at different orientation. This clearly indicates the overlap of two disintegrated LSM particles. Also, the abrupt image contrast change at the LSM/YSZ interface is most likely due to the strain effect resulted from the lattice mismatch of the heterogeneous phases[60-63]. The mismatch strain and the lattice misfit are usually relaxed and accommodated by the occurrence of misfit dislocations [64-66], e.g. lattice plane distortion and bending at the interface, as indicated in Fig. 7.

3.5 LSM/GDC interface

The influence of cathodic polarization on the interface of directly assembled LSM/GDC electrodes was also investigated and the results are shown in Fig.8. Different to that observed on the LSM/YSZ electrode, no Mn segregation was observed after polarization at 900 ^{o}C and 500 mAcm^{-2} for 1 h (Fig. 8a). An intimate LSM/GDC interface was established with a high level of periodicity and symmetry, free of voids and amorphous phases (Fig.8b). The GDC electrolyte is characterized by $\{111\}_{GDC}$ planes with plane spacing of 0.31 nm, while LSM cathode can be identified by $\{110\}_{LSM}$ lattice planes with plane spacing of 0.27 nm. The orientation relationship of these two planes was $\theta_{\{111\}GDC/\{110\}LSM} = 11.0^{o}$ with $f = 12.9\%$. Similar to the LSM/YSZ interface, the lattice plane distortion was also observed (indicated by the red arrows in Fig. 8b). Nevertheless, the observed lattice distortion only existed locally at the interface region without propagating into the electrode or electrolyte bulk.

The directly assembled LSM on GDC electrolyte was also polarized at 900 ^{o}C and 500 mAcm^{-2} for 12 h. LSM particles were in good contact with GDC electrolyte and there was no disintegration of LSM phase at the interface (Fig.9a), very different to that observed on LSM/YSZ electrode under the identical polarization conditions (Fig.7). However, similar to LSM/YSZ electrodes, Mn segregation from the LSM perovskite was observed. The polarization induced LSM/GDC interface is sharp and characterized by a high symmetry of lattice plane structure for both LSM and GDC phases (see Fig. 9b). From the FFT diffractogram images, the GDC electrolyte phase can be identified by its $\{220\}_{GDC}$ lattice planes with plane spacing of 0.19 nm, while LSM phase by the $\{012\}_{LSM}$ and $\{024\}_{LSM}$ planes with plane spacing of 0.39 nm and 0.19 nm, respectively. The orientation relationship of $\{220\}_{GDC}$ and $\{024\}_{LSM}$ was found to be 14.7^{o} with lattice mismatch factor of 13%. The much stable LSM/GDC interface may indicate that the solubility of La^{3+} and Mn^{2+} in GDC is much lower than that in YSZ[55, 57, 67, 68].

Mn segregation from the LSM perovskite structure occurs in both LSM/YSZ and LSM/GDC electrodes under SOFC polarization conditions. Fig.10 presents typical STEM-EDS element mapping and HRTEM analysis of the interface between segregated manganese oxide (MnO_x) and LSM electrode on GDC electrolyte after polarization at 900 ^oC and 500 $mAcm^{-2}$ for 12 h. The segregation of MnO_x was indicated by the $\{013\}_{MnOx}$ and $\{111\}_{MnOx}$ planes with corresponding lattice plane spacing of 0.29 nm and 0.25 nm, respectively (Fig.10b). The MnO_x particle is in an intimate contact with LSM electrode, free of voids or other phases, characterized by a high level of symmetry and periodicity in lattice plane arrangement at the interface. The interface geometry of MnO_x/LSM was revealed as the matching of $\{111\}_{MnOx}$ and $\{110\}_{LSM}$ lattice planes with an orientation relationship of $\theta_{\{111\}MnOx/\{110\}LSM} = 40.7^o$ and a mismatch factor of 7.4%. The influence of Mn segregation on the performance degradation of the LSM/YSZ and LSM/GDC cells is not clear at this stage. However, MnO_x has a low electronic conductivity. The segregated MnO_x, if diffuses at the TPB, would partially block the transfer of electrons thus the increase of contact resistance might be expected, which would lead to the degradation of LSM electrode.

3.6 Effect of polarization on the interface formation and Mn segregation

The results shown in the present study clearly indicate the significant effect of cathodic polarization on the interface formation and Mn segregation of directly assembled LSM/YSZ and LSM/GDC electrodes. The findings on the cathode/electrolyte interface microstructure and Mn segregation is summarized below:

1. For directly assembled LSM/YSZ electrode, there is a significant change in the microstructure and morphology of the YSZ electrolyte surface in contact with LSM electrode, indicated by the disintegration of LSM particles and formation of ring-shaped craters. With the increase of the polarization time, the contact rings continue to grow in

size, and the disintegration of the LSM particle becomes much more obvious at the interface, resulting in the formation of La-Mn-Zr solid solution. The results indicate the establishment of an intimate interface and the atomic geometry of the LSM/YSZ interface is characterized by the matching of $\{202\}_{LSM}$ and $\{111\}_{YSZ}$ or $\{220\}_{YSZ}$ lattice planes with a mismatch factor of 18.2-24.1%. The significantly enhanced electrochemical performance with the cathodic polarization demonstrates that the disintegrated LSM particles at the LSM/YSZ interface do not significantly impede the oxygen reduction process.

2. In the case of directly assembled LSM/GDC electrode, the change in the microstructure and morphology of GDC electrolyte is much smaller, very different from the substantial microstructure changes observed for the LSM/YSZ electrodes under the identical polarization conditions. Disintegration of LSM particles at the interface was not observed. The polarization induced LSM/GDC interface is indicated by the formation of small and shallow contact marks, and characterized by the matching of $\{024\}_{LSM}$ and $\{220\}_{GDC}$ or $\{110\}_{LSM}$ and $\{111\}_{GDC}$ lattice planes with a mismatch factor in the range of 1.3% to 12.9%. As compared to the LSM/YSZ electrode, the LSM/GDC interface is quite stable under polarization conditions, which is in good agreement with that reported in the literature[67]. Electrochemically, LSM/GDC electrode behaves similarly to that of LSM/YSZ electrode, showing the significantly reduced polarization and ohmic resistance with the polarization, though the magnitude in the change of the polarization resistances is relatively smaller (see Fig.1).
3. The significantly enhanced electrochemical performance of LSM electrodes during the cathodic polarization indicates that the presence of misfit dislocations and distortions at the interface does not impede the migration and incorporation of O^{2-} from the LSM cathode into the electrolyte at the three phase boundary region. This is consistent with

that reported in the literature [22, 37, 69]. For example, Pergolesi *et al*.[69] fabricated CeO_2 and YSZ biaxially textured epitaxial thin film using pulsed laser deposition method, and found that the hetero-interfaces were not uniform but significantly strained, yet no detectable contribution to the oxygen transport properties was found.

4. For both LSM/YSZ and LSM/GDC electrodes, Mn segregation from the cathode was observed under the influence of the cathodic polarization. The segregated Mn particle most likely exists as MnO_x, and does not show preferential deposition at the interface, indicating that the segregated Mn would not diffuse to the cathode/electrolyte interface during the oxygen reduction process. The observed MnO_x/LSM interface is sharp and clean without any noticeable voids or amorphous phase. The atomic geometry of the examined interface can be identified by the matching of $\{111\}_{MnOx}$ and $\{110\}_{LSM}$ lattice planes with a mismatch factor of 7.4%.

Mn segregation has been commonly observed on the LSM electrodes under SOFC operation conditions. Chen *et al*.[70] studied the interface reactions between LSM cathode and YSZ electrolyte in different atmospheres at 1000 ^oC and found that Mn segregation was more pronounced at low oxygen partial pressure. This is consistent with that reported by Nishiyama [71], in which the oxygen potential gradient developed in the manganite was considered to give rise to the similar gradients in chemical potential of manganese, providing a driving force for manganese oxide segregation at the surface. Liu *et al*.[72] studied the influence of water vapour on the degradation behaviour of LSM based cells and observed an enrichment of Mn_2O_3 and Mn_3O_4 nano-particles (~100 nm in size) on the electrode surface by STEM-EDS mapping after the cell was exposed to 20 vol.% humidified air and operated at 800 ^oC for 200 h. We also observed a clear formation of Mn-rich phase, possibly Mn_3O_4 in the LSM electrode after the LSM-YSZ based cell was subject to a current load of 500 $mAcm^{-2}$ at 1000 ^oC for 2543 h[73].

Liu *et al*.[74] reported that Mn segregation occurred for the LSM-YSZ composite cathode and YSZ electrolyte after polarization at 850 ^{o}C and 1.76 Acm^{-2} for 1500 h, and proposed that the Mn migration cannot be simply attributed to the element diffusion. For perovskite-type LSM, the electrical neutrality due to substitution of La^{3+} by Sr^{2+} at the A site is maintained by a change in Mn valence. Lee *et al.* investigated active sites for O_2 reduction in the LSM electrode under various cathodic polarization potentials using *in situ* X-ray photoelectron spectroscopy (XPS) and observed a shifting of the Mn 2p peaks to the lower binding energy side as the applied potential became more cathodic[75]. A recent study by Traulsen *et al*.[76] using operando X-ray absorption spectroscopy techniques showed that cathodic polarizations induced a shift in the Mn K edge energy towards lower energies due to a decrease in the average Mn oxidation state. This suggests the valence change of Mn ions in the lattice and interstitial sites under cathodic polarization. The valence change of Mn ions in the perovskite can cause the structural change and segregation of Mn species to the electrode and electrolyte surface[77, 78]. The segregation of Mn species under cathodic polarization conditions has also been suggested as the main nucleation agents for the deposition of Cr on LSM electrodes under SOFC operation conditions[79, 80].

The current study demonstrates that nature of electrolyte has a significant effect on the stability of the LSM/electrolyte interface. LSM on GDC electrolyte shows a much more stable interface than that of LSM on YSZ electrolyte under identical polarization conditions. Due to the fact that the directly assembled electrodes do not go through the high temperature sintering, the initial physical contact between LSM electrode with YSZ or GDC electrolyte is very weak. Consequently, the low contact area would result in the initial high contact resistance (*i.e.*, R_{Ω}), 2.1 Ω cm^2 in the case of LSM/YSZ electrode and 1.0 Ω cm^2 in the case of LSM/GDC electrode. The high ohmic resistance will result in a much higher local current density at the interface, leading to the localized sintering due to the Joule heating. The heat generated will sinter the

interface and thus enhance the contacts at the interface. This explains the significant reductions in R_Ω after polarization at 900 ^oC and 500 $mAcm^{-2}$ for 12 h from 2.1 to 0.9 $\Omega\ cm^2$ on LSM/YSZ electrode and from 1.0 $\Omega\ cm^2$ to 0.3 $\Omega\ cm^2$ on LSM/GDC electrode (Fig.1). However, the observed disintegration of LSM particles at the LSM/YSZ interface indicates that the heat generated at the LSM/YSZ interface would be significantly higher than that at the LSM/GDC interface. The underlying reason for the differences in the localized heating at the interface is most likely related to the significant differences in the ionic and electronic conducting properties of YSZ and GDC materials. YSZ is a pure oxygen ion conductor with the ionic conductivity in 0.08-0.11 S/cm range at 1000 ^oC [81, 82], while the doped ceria, such as GDC, is a mixed ionic and electronic conductor with significantly higher conductivities (0.20-0.25 S/cm at 1000 ^oC) [83, 84]. The high ionic conductivity and mixed ionic and electronic conducting properties of GDC could reduce the electrode ohmic resistance and at the same time accelerate the oxygen migration and diffusion at the interface between LSM and GDC. The electronic conductivity of GDC becomes significant at low oxygen partial pressure and high operating temperature (>800^oC) [85, 86], therefore the electronic current in GDC can occur, which may also influence the reaction at the LSM/GDC interface. This is in fact supported by the much lower R_Ω and R_p values of the LSM/GDC electrode, as compared to that measured on LSM/YSZ electrodes before polarization (see Fig.1).

Fig. 11 shows a schematic diagram to compare the Mn diffusion and interface formation in pre-sintered[22] and directly assembled LSM/YSZ and LSM/GDC electrodes in this study. For the pre-sintered LSM/YSZ cell, the interface establishment after high temperature sintering is characterised by the formation of convex contact rings on the electrolyte, and the atomic geometry of the intimate electrode/electrolyte interface can be identified by a high level of symmetry, free of voids and amorphous phases (Fig.11a). In addition, Mn^{2+} and La^{3+} cation diffuse towards the YSZ electrolyte and cation accumulation in the convex contact rings were

observed, indicating a strong solubility of La^{3+} and in particular Mn^{2+} species in YSZ. Similar to the LSM/YSZ electrodes, the pre-sintered LSM/GDC interface is also characterised by the formation of convex contact rings on the GDC electrolyte surface. No cation diffusion is detected due to their low solubility in doped ceria. This is in good agreement with the chemical equilibrium calculations reported in the literature [87]. In $(ZrO_2)_{0.85}(YO_{1.5})_{0.15}$ at 1000 ^oC, the calculated solubility of manganese is 5.1 %, (1.4% as Mn^{3+} and 3.7% as Mn^{2+}). A detailed experimental investigation of the ternary phase diagram of $(Zr,Y)O_2$-La_2O_3-Mn_3O_4 at 1400 ^oC showed that the solubility of manganese in cubic zirconia solid solution phase was between 15 and 25 mol%[57]. In contrast, no solid solution was observed in MnO-Mn_2O_3-CeO_2 system above 800 ^oC. As the Mn segregation is most likely caused by the valence change of Mn ions in the perovskite structure under cathodic polarization conditions[75, 76], this also explains the observation that no MnO_x segregation occurs on pre-sintered LSM/YSZ and LSM/GDC electrodes (see Fig.11a)[22]. In the case of the directly assembled LSM/YSZ and LSM/GDC electrodes, the formation of an intimate electrode/electrolyte interface was also observed under the cathodic polarization conditions (Fig.11b). The significant differences in the microstructure and morphology of the electrode/electrolyte interface can be attributed to the significant differences in the nature of YSZ and GDC electrolyte materials as discussed above.

5. Conclusion

The interface formation and Mn segregation and diffusion of directly assembled LSM/YSZ and LSM/GDC electrodes were studied under cathodic polarization conditions at 900 ^oC using combined FIB-STEM techniques. The results indicate that in the case of both LSM/YSZ and LSM/GDC electrodes, the cathodic current passage induces the formation of intimate electrode/electrolyte interface, indicated by the significant reduction in both R_p and R_Ω. However, the change in the YSZ electrolyte surface in contact with LSM electrode is substantial, as compared to that on GDC electrolyte, characterized by the disintegration of LSM

phase at the electrode/electrolyte interface and the formation of ring-shaped contact craters at the interface. The main reason for the disintegration of LSM phase at the interface is due to the much higher localized heat generated at the interface due to the low ionic conductivity of YSZ electrolyte material in comparison to that of GDC electrolyte. In addition, Mn segregation was observed for both LSM/YSZ and LSM/GDC electrodes under the effect of cathodic polarization, and the segregated MnO_x does not show preferential deposition at the interface. This is probably the main reason for the negligible detrimental effect of segregated MnO_x on the electrochemical activity of LSM electrode studied in this work. This study provides an insight in the fundamental understanding of electrode/electrolyte interface formation and Mn segregation in relation to the nature of electrolyte of SOFCs and has significant implications in the development of active and stable cathodes of SOFCs in general.

Acknowledgment

This work was financially supported by the Australian Research Council under the Discovery Project Scheme (project number: DP180100731 and DP180100568), and by the Guangdong Provincial Department of Science and Technology Agency (GDST) under the GDST-NOW Science-Industry Coorperation Program (No.2017A050501053). The authors acknowledge the facilities and the scientific and technical assistance of Curtin University Microscopy & Microanalysis Facility and the Australian Microscopy & Microanalysis Research Facility at the Centre for Microscopy, Characterization & Analysis, The University of Western Australia, a facility funded by the University, State and Commonwealth Governments, and the Key Laboratory of Precision Microelectronic Manufacturing Technology & Equipment of Ministry of Education of China.

References:

[1] T.M. Gür, *Progress in Energy and Combustion Science* **54** (2016) 1.

[2] A. Choudhury, H. Chandra, A. Arora, *Renewable and Sustainable Energy Reviews* **20** (2013) 430.
[3] K. Chen, L. Zhang, N. Ai, S. Zhang, Y. Song, Y. Song, Q. Yi, C.-Z. Li, S.P. Jiang, *Energy & Fuels* (2015).
[4] D. Papurello, R. Borchiellini, P. Bareschino, V. Chiodo, S. Freni, A. Lanzini, F. Pepe, G.A. Ortigoza, M. Santarelli, *Applied Energy* **125** (2014) 254.
[5] S.Y. Wang, S.P. Jiang, *National Science Review* **4** (2017) 163.
[6] N. Mahato, A. Banerjee, A. Gupta, S. Omar, K. Balani, *Progress in Materials Science* **72** (2015) 141.
[7] S.C. Singhal, *Wiley Interdisciplinary Reviews: Energy and Environment* **3** (2014) 179.
[8] H. Moon, S. Kim, S. Hyun, H. Kim, *International Journal of Hydrogen Energy* **33** (2008) 1758.
[9] T. Fukui, S. Ohara, M. Naito, K. Nogi, *Journal of Power Sources* **110** (2002) 91.
[10] S.P. Jiang, *Journal of Materials Science* **43** (2008) 6799.
[11] M. Backhausricoult, *Solid State Ionics* **177** (2006) 2195.
[12] Y.L. Liu, A. Hagen, R. Barfod, M. Chen, H.J. Wang, F.W. Poulsen, P.V. Hendriksen, *Solid State Ionics* **180** (2009) 1298.
[13] J.T.S. Irvine, D. Neagu, M.C. Verbraeken, C. Chatzichristodoulou, C. Graves, M.B. Mogensen, *Nature Energy* **1** (2016) 15014.
[14] T. Matsui, Y. Mikami, H. Muroyama, K. Eguchi, *J. Electrochem. Soc.* **157** (2010) B1790.
[15] S. Jiang, J.G. Love, L. Apateanu, *Solid State Ionics* **160** (2003) 15.
[16] A. Belzner, T. Gur, R. Huggins, *Solid State Ionics* **57** (1992) 327.
[17] T. Horita, T. Tsunoda, K. Yamaji, N. Sakai, T. Kato, a.H. Yokokawa, *Solid State Ionics* **152-153** (2002) 439.
[18] S.P. Jiang, W. Wang, *Electrochemical and Solid-State Letters* **8** (2005) A115.
[19] T. Matsui, Y. Mikami, H. Muroyama, K. Eguchi, *Journal of Power Sources* **242** (2013) 790.
[20] B. Hu, M. Keane, M.K. Mahapatra, P. Singh, *Journal of Power Sources* **248** (2014) 196.
[21] T. Matsui, M. Komoto, H. Muroyama, K. Eguchi, *Fuel Cells* **14** (2014) 1022.
[22] S. He, K.F. Chen, M. Saunders, J. Li, C.Q. Cui, S.P. Jiang, *J. Electrochem. Soc.* **164** (2017) F1437.
[23] J. Yang, H. Muroyama, T. Matsui, K. Eguchi, *Journal of Power Sources* **204** (2012) 25.
[24] M.J. Jørgensen, P. Holtappels, C.C. Appel, *Journal of Applied Electrochemistry* **30** (2000) 411.
[25] M.A. Haider, S. McIntosh, *Journal of The Electrochemical Society* **156** (2009).
[26] G.J. la O, R.F. Savinell, Y. Shao-Horn, *J. Electrochem. Soc.* **156** (2009) B771.
[27] K. Chen, S.S. Liu, N. Ai, M. Koyama, S.P. Jiang, *Phys Chem Chem Phys* **17** (2015) 31308.
[28] S.P. Jiang, *Journal of The Electrochemical Society* **162** (2015) F1119.
[29] K. Chen, N. Li, N. Ai, Y. Cheng, W.D. Rickard, S.P. Jiang, *ACS Appl Mater Interfaces* **8** (2016) 31729.
[30] M. Li, K. Chen, B. Hua, J.-l. Luo, W.D.A. Rickard, J. Li, J.T.S. Irvine, S.P. Jiang, *Journal of Materials Chemistry A* **4** (2016) 19019.
[31] N. Li, N. Ai, K. Chen, Y. Cheng, S. He, M. Saunders, A. Dodd, A. Suvorova, S.P. Jiang, *RSC Adv.* **6** (2016) 99211.
[32] N. Ai, N. Li, S. He, Y. Cheng, M. Saunders, K. Chen, T. Zhang, S.P. Jiang, *J. Mater. Chem. A* **5** (2017) 12149.
[33] N. Ai, N. Li, W.D. Rickard, Y. Cheng, K. Chen, S.P. Jiang, *ChemSusChem* **10** (2017) 993.
[34] N. Ai, S. He, N. Li, Q. Zhang, W.D.A. Rickard, K. Chen, T. Zhang, S.P. Jiang, *Journal of Power Sources* **384** (2018) 125.
[35] N. Li, N. Ai, S. He, Y. Cheng, W.D.A. Rickard, K. Chen, T. Zhang, S.P. Jiang, *Solid State Ionics* **316** (2018) 38.
[36] K. Chen, S. He, N. Li, Y. Cheng, N. Ai, M. Chen, W.D.A. Rickard, T. Zhang, S.P. Jiang, *Journal of Power Sources* **378** (2018) 433.
[37] S. He, M. Saunders, K. Chen, H. Gao, A. Suvorova, W.D.A. Rickard, Z. Quadir, C.Q. Cui, S.P. Jiang, *Journal of The Electrochemical Society* **165** (2018) F417.

[38] K. Chen, N. Li, N. Ai, M. Li, Y. Cheng, W.D.A. Rickard, J. Li, S.P. Jiang, *Journal of Materials Chemistry A* **4** (2016) 17678.
[39] S.P. Jiang, *Journal of Solid State Electrochemistry* **11** (2005) 93.
[40] S. Jiang, J. Love, *Solid State Ionics* **138** (2001) 183.
[41] W. Wang, S.P. Jiang, *Solid State Ionics* **177** (2006) 1361.
[42] M.A. Haider, S. McIntosh, *J. Electrochem. Soc.* **156** (2009) B1369.
[43] A.A. Vance, S. McIntosh, *J. Electrochem. Soc.* **155** (2008) B1.
[44] A.J. McEvoy, *Solid State Ionics* **135** (2000) 331.
[45] M.L. Liu, Z.L. Wu, *Solid State Ionics* **107** (1998) 105.
[46] B. Philippeau, F. Mauvy, C. Mazataud, S. Fourcade, J.C. Grenier, *Solid State Ionics* **249** (2013) 17.
[47] R. Moriche, D. Marrero-López, F.J. Gotor, M.J. Sayagués, *Journal of Power Sources* **252** (2014) 43.
[48] A. Hammouche, E. Siebert, A. Hammou, *Materials Research Bulletin* **24** (1989) 367.
[49] C.M. Wang, S. Azad, V. Shutthanandan, D.E. McCready, C.H.F. Peden, L. Saraf, S. Thevuthasan, *Acta Materialia* **53** (2005) 1921.
[50] D. Wolf, S. Yip, *Materials Interfaces: Atomic-level Structure and Properties*, Springer Netherlands (1993).
[51] S. Cazottes, Z.L. Zhang, R. Daniel, J.S. Chawla, D. Gall, G. Dehm, *Thin Solid Films* **519** (2010) 1662.
[52] Y. Ikuhara, *Journal of the Ceramic Society of Japan* **109** (2001) S110.
[53] J.P. Locquet, D. Neerinck, L. Stockman, Y. Bruynseraede, I.K. Schuller, *Physical Review B* **38** (1988) 3572.
[54] Tatsuya Kawada, Natsuko Sakai, Harumi Yokokawa, M. Dokiya, *Solid State Ionics* **50** (1992) 189.
[55] M. Mori, T. Abe, H. Itoh, O. Yamamoto, G.Q. Shen, Y. Takeda, N. Imanishi, *Solid State Ionics* **123** (1999) 113.
[56] S.P. Simner, J.P. Shelton, M.D. Anderson, J.W. Stevenson, *Solid State Ionics* **161** (2003) 11.
[57] S.P. Jiang, J.P. Zhang, K. Foger, *J. Eur. Ceram. Soc.* **23** (2003) 1865.
[58] A. Mitterdorfer, L.J. Gauckler, *Solid State Ionics* **111** (1998) 185.
[59] U. Martin, H. Boysen, F. Frey, *Acta Crystallographica Section B Structural Science* **49** (1993) 403.
[60] O.I. Lebedev, G.V. Tendeloo, S. Amelinckx, H.L. Ju, K.M. Krishnan, *Philosophical Magazine A* **80** (2000) 673.
[61] C. Rentenberger, C. Mangler, S. Scheriau, R. Pippan, H.P. Karnthaler, *Materials Science Forum* **584-586** (2008) 422.
[62] X.L. Wu, E. Ma, *Journal of Materials Research* **22** (2011) 2241.
[63] M. Sillassen, P. Eklund, N. Pryds, E. Johnson, U. Helmersson, J. Bøttiger, *Advanced Functional Materials* **20** (2010) 2071.
[64] F.K. LeGoues, *MRS Bulletin* **21** (1996) 38.
[65] F. Ernst, P. Pirouz, A.H. Heuer, *Philosophical Magazine A* **63** (1991) 259.
[66] A. Trampert, F. Ernst, C.P. Flynn, H.F. Fischmeister, M. Ru¨hle, *Acta Metallurgica et Materialia* **40** (1992) S227.
[67] L. Zhao, J. Hyodo, T. Ishihara, K. Sasaki, S.R. Bishop, *ECS Transactions* **57** (2013) 1607.
[68] V.P. Dravid, V. Ravikumar, M.R. Notis, C.E. Lyman, G. Dhalenne, A. Revcolevschi, *Journal of the American Ceramic Society* **77** (1994) 2758.
[69] D. Pergolesi, E. Fabbri, S.N. Cook, V. Roddatis, E. Traversa, J.A. Kilner, *ACS Nano* **6** (2012) 10524.
[70] M. Chen, Y.L. Liu, A. Hagen, P.V. Hendriksen, F.W. Poulsen, *Fuel Cells* **9** (2009) 833.
[71] H. Nishiyama, *Journal of The Electrochemical Society* **143** (1996).

[72] R.R. Liu, S.H. Kim, S. Taniguchi, T. Oshima, Y. Shiratori, K. Ito, K. Sasaki, *J. Power Sources* **196** (2011) 7090.
[73] S. Jiang, W. Wang, *Solid State Ionics* **176** (2005) 1185.
[74] Y.L. Liu, K. Thyden, M. Chen, A. Hagen, *Solid State Ionics* **206** (2012) 97.
[75] H.Y. Lee, W.S. Cho, S.M. Oh, H.D. Wiemhofer, W. Gopel, *J. Electrochem. Soc.* **142** (1995) 2659.
[76] M.L. Traulsen, H.W.P. de Carvalho, P. Zielke, J.D. Grunwaldt, *J. Electrochem. Soc.* **164** (2017) F3064.
[77] S.P. Jiang, J.G. Love, *Solid State Ionics* **158** (2003) 45.
[78] M. Backhaus-Ricoult, K. Adib, T.S. Clair, B. Luerssen, L. Gregoratti, A. Barinov, *Solid State Ionics* **179** (2008) 891.
[79] S.P. Jiang, J.P. Zhang, L. Apateanu, K. Foger, *J. Electrochem. Soc.* **147** (2000) 4013.
[80] S.P. Jiang, S. Zhang, Y.D. Zhen, *J. Mater. Res.* **20** (2005) 747.
[81] X.J. Chen, K.A. Khor, S.H. Chan, L.G. Yu, *Materials Science and Engineering: A* **335** (2002) 246.
[82] S.P.S. Badwal, *Solid State Ionics* **52** (1992) 23.
[83] K. Eguchi, T. Setoguchi, T. Inoue, H. Arai, *Solid State Ionics* **52** (1992) 165.
[84] H. Inaba, *Solid State Ionics* **83** (1996) 1.
[85] S. Lübke, H.D. Wiemhöfer, *Berichte der Bunsengesellschaft für physikalische Chemie* **102** (1998) 642.
[86] S. Wang, T. Kobayashi, M. Dokiya, T. Hashimoto, *Journal of The Electrochemical Society* **147** (2000).
[87] Rober S. Roth, T.A. Vanderah, *Phase Equilibria Diagrams - Volume XIV: Oxides*, American Ceramic Society, U.S. (2005).

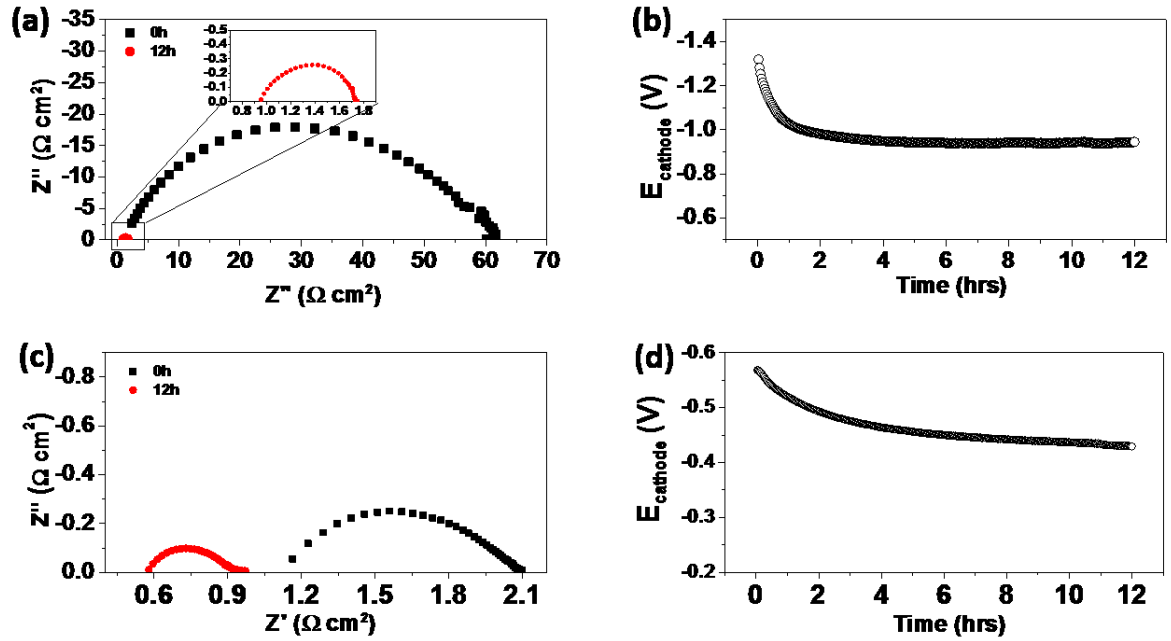

Figure 1. Electrochemical performance of directly assembled LSM cathode on (a,b) YSZ and (c,d) GDC electrolytes before and after polarization at 900 ^{o}C and 500 mAcm^{-2} for 12 h.

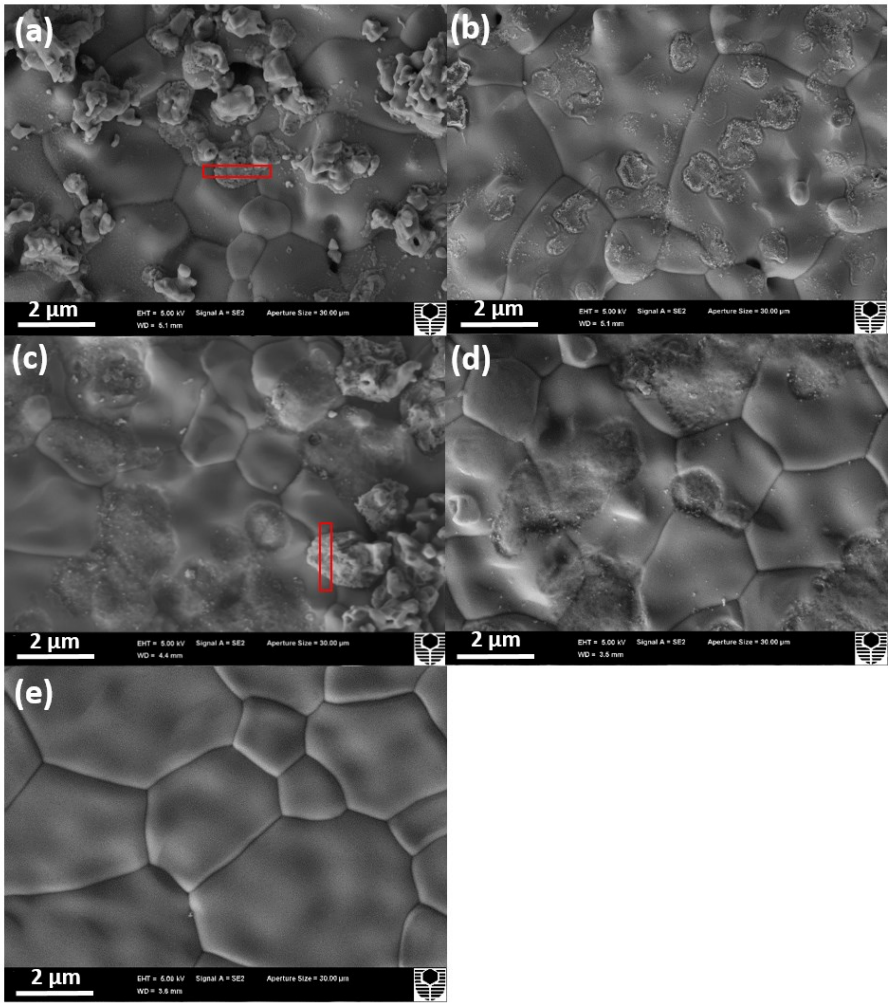

Figure 2. SEM micrographs of YSZ electrolyte surface after polarization at 900°C and 500 $mAcm^{-2}$ for (a,b) 1 h and (c,d) 12 h. The LSM electrodes were removed (a,c) by stick tape and (b,d) by HCl treatment. The original YSZ electrolyte surface without LSM coating is given in (e). The red boxes indicate the locations of FIB milling.

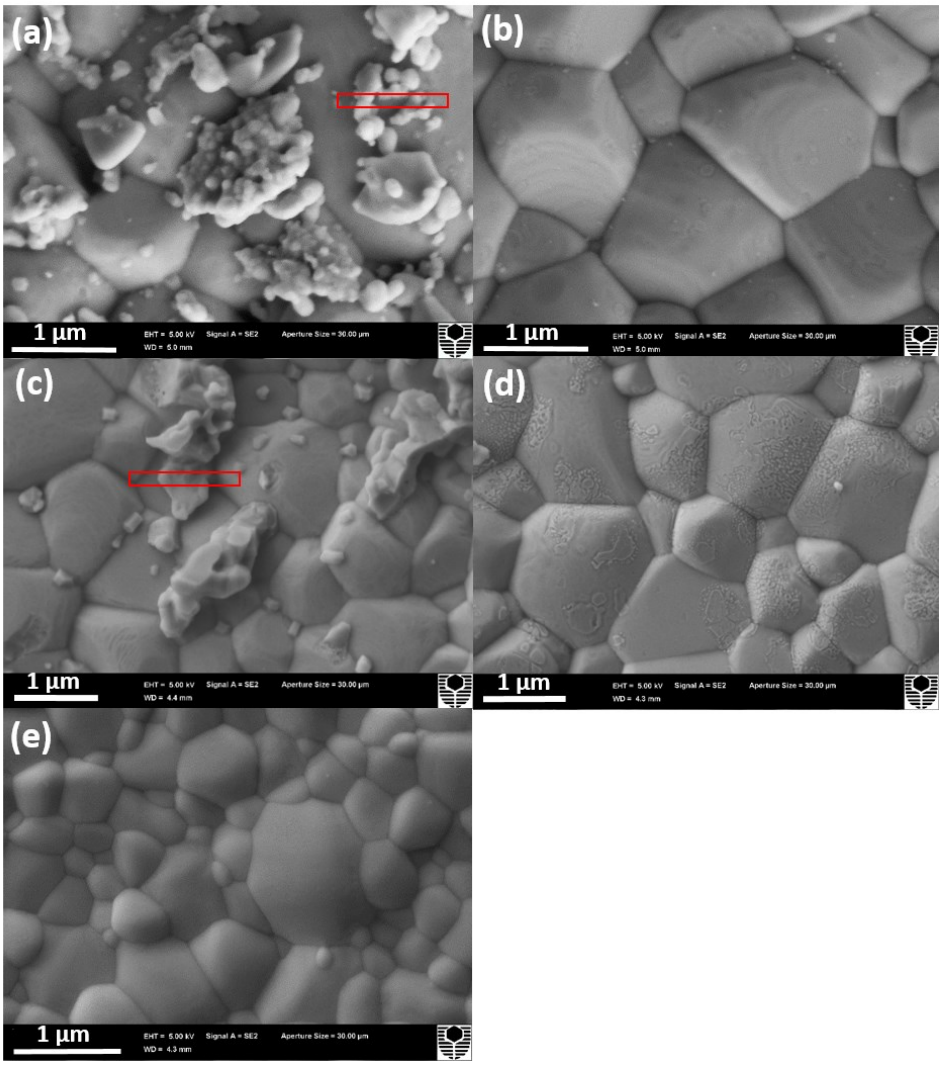

Figure 3. SEM micrographs of GDC electrolyte surface after polarization at 900°C and 500 $mAcm^{-2}$ for (a,b) 1 h and (c,d) 12 h. The LSM electrodes were removed (a,c) by stick tape and (b,d) by HCl treatment. The original GDC electrolyte surface without LSM coating is given in (e). The red boxes indicate the locations of FIB milling.

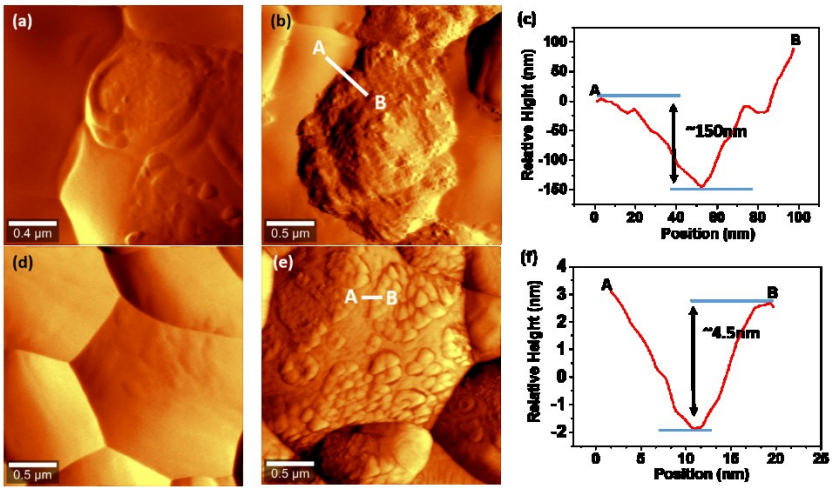

Figure 4. AFM micrographs and line scan of (a,b,c) YSZ and (d,e,f) GDC electrolyte surfaces in contact with LSM electrode after polarization at 900°C and 500 $mAcm^{-2}$ for (a,d) 1 h and (b,e) 12 h. The LSM cathode was removed by HCl treatment.

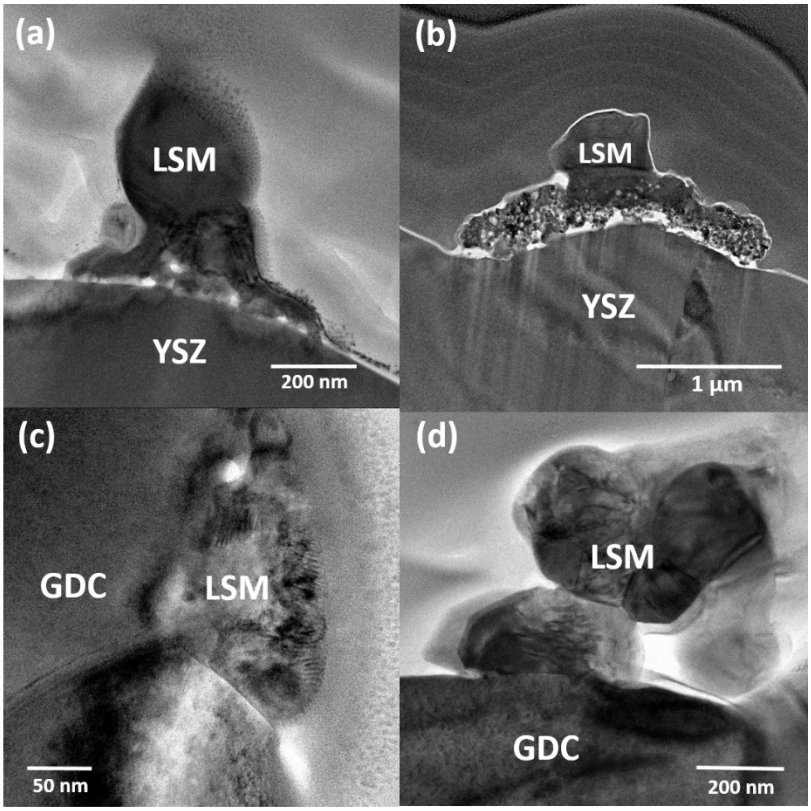

Figure 5. TEM micrographs of (a,b) LSM/YSZ interface and (c,d) LSM/GDC interface after polarization at 900 ºC and 500 $mAcm^{-2}$ for (a,c) 1 h and (b,d) 12 h.

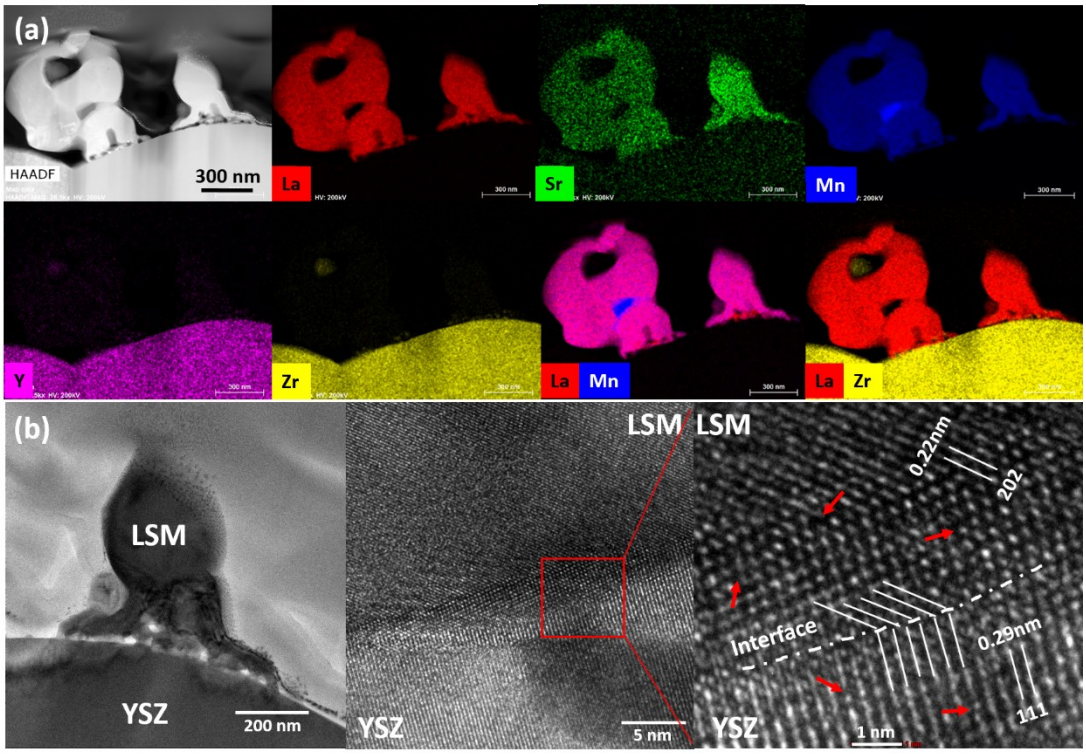

Figure 6. (a) STEM-EDS element mapping and (b) HRTEM micrographs of directly assembled LSM cathode on YSZ electrolyte after polarization at 900°C and 500 $mAcm^{-2}$ for 1 h. The red arrows indicate the locations of lattice distortion.

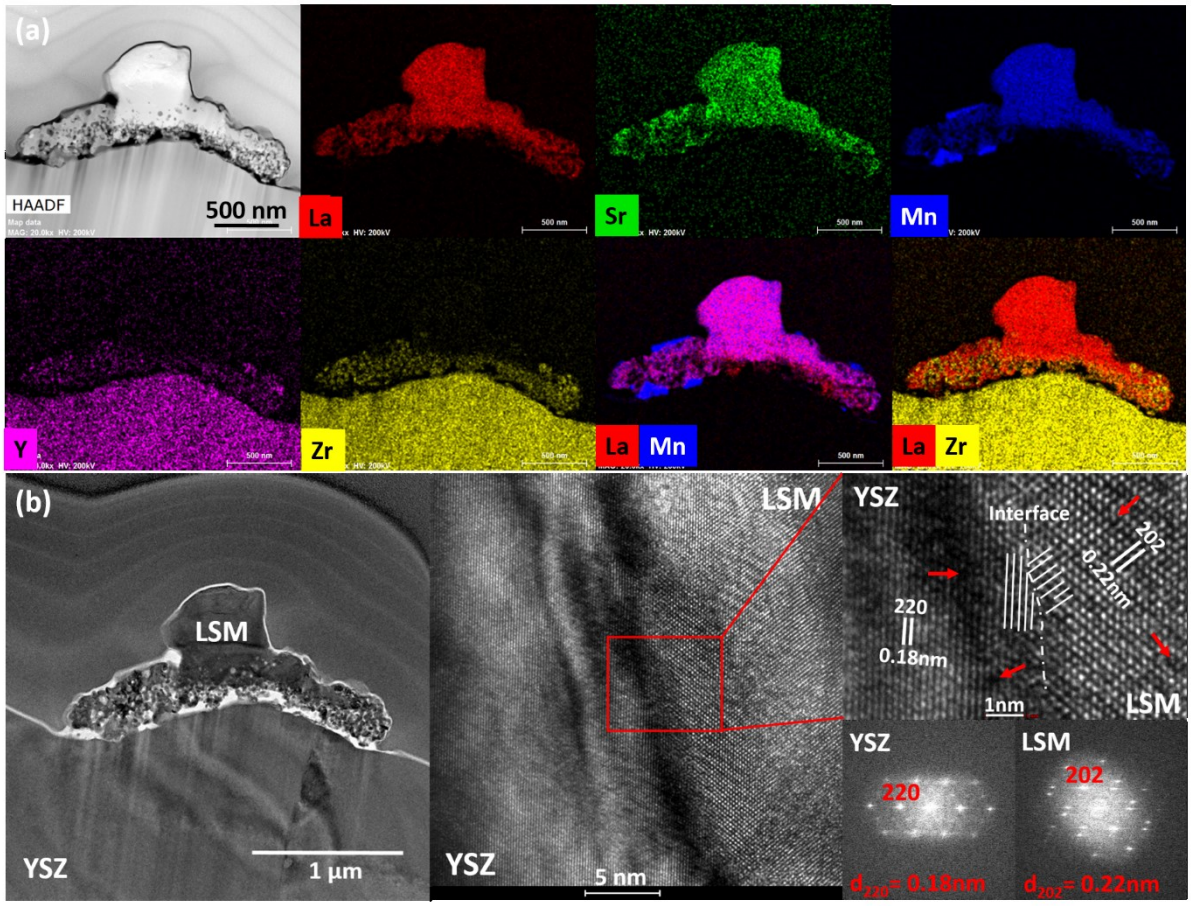

Figure 7. (a) STEM-EDS element mapping and (b) HRTEM micrographs of directly assembled LSM cathode on YSZ electrolyte after polarization at 900 ^{o}C and 500 mAcm^{-2} for 12 h. The FFT shows the diffractograms of the YSZ and LSM phases. The red arrows indicate the locations of lattice distortion.

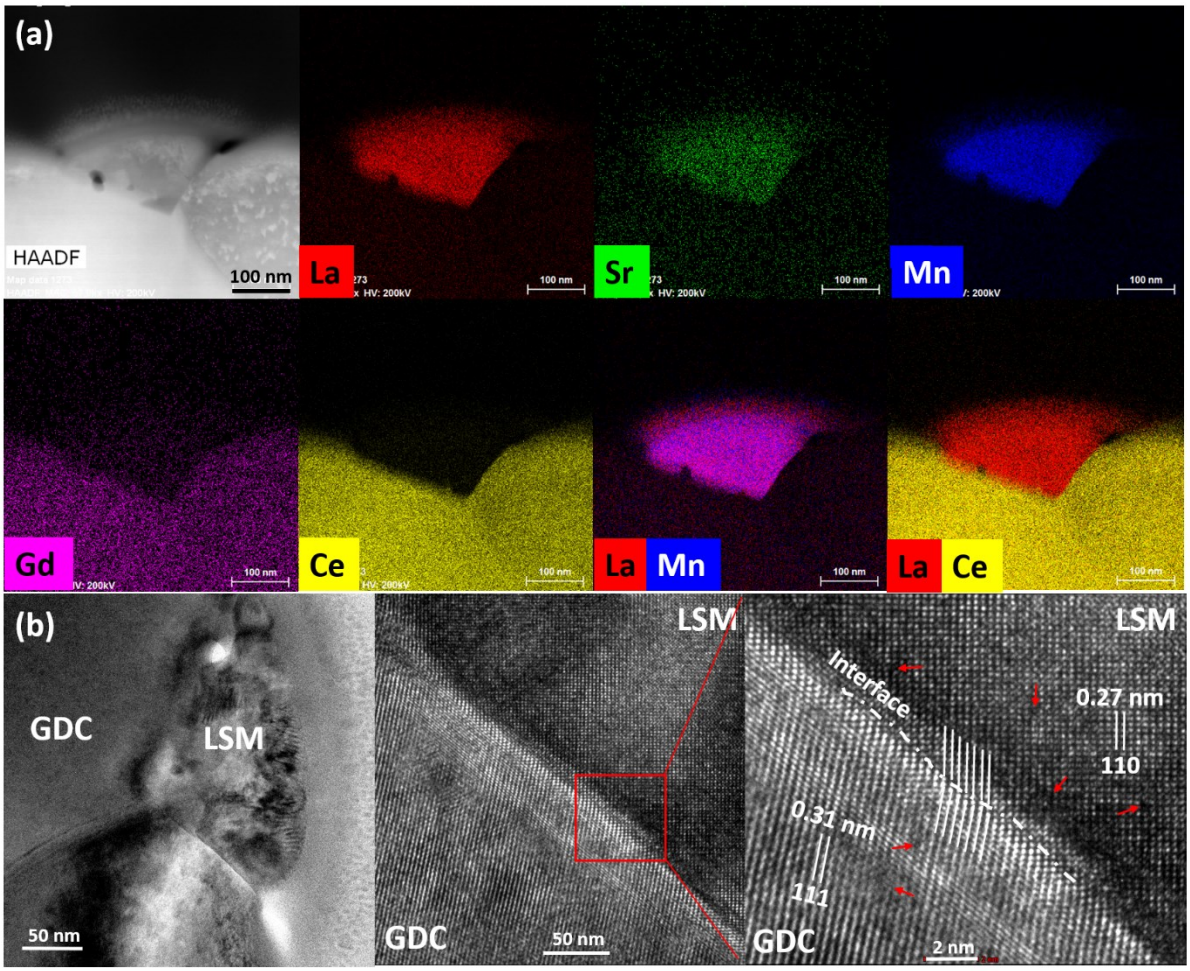

Figure 8. (a) STEM-EDS element mapping and (b) HRTEM micrographs of directly assembled LSM cathode on GDC electrolyte after polarization at 900ºC and 500 $mAcm^{-2}$ for 1 h. The red arrows indicate the locations of lattice distortion.

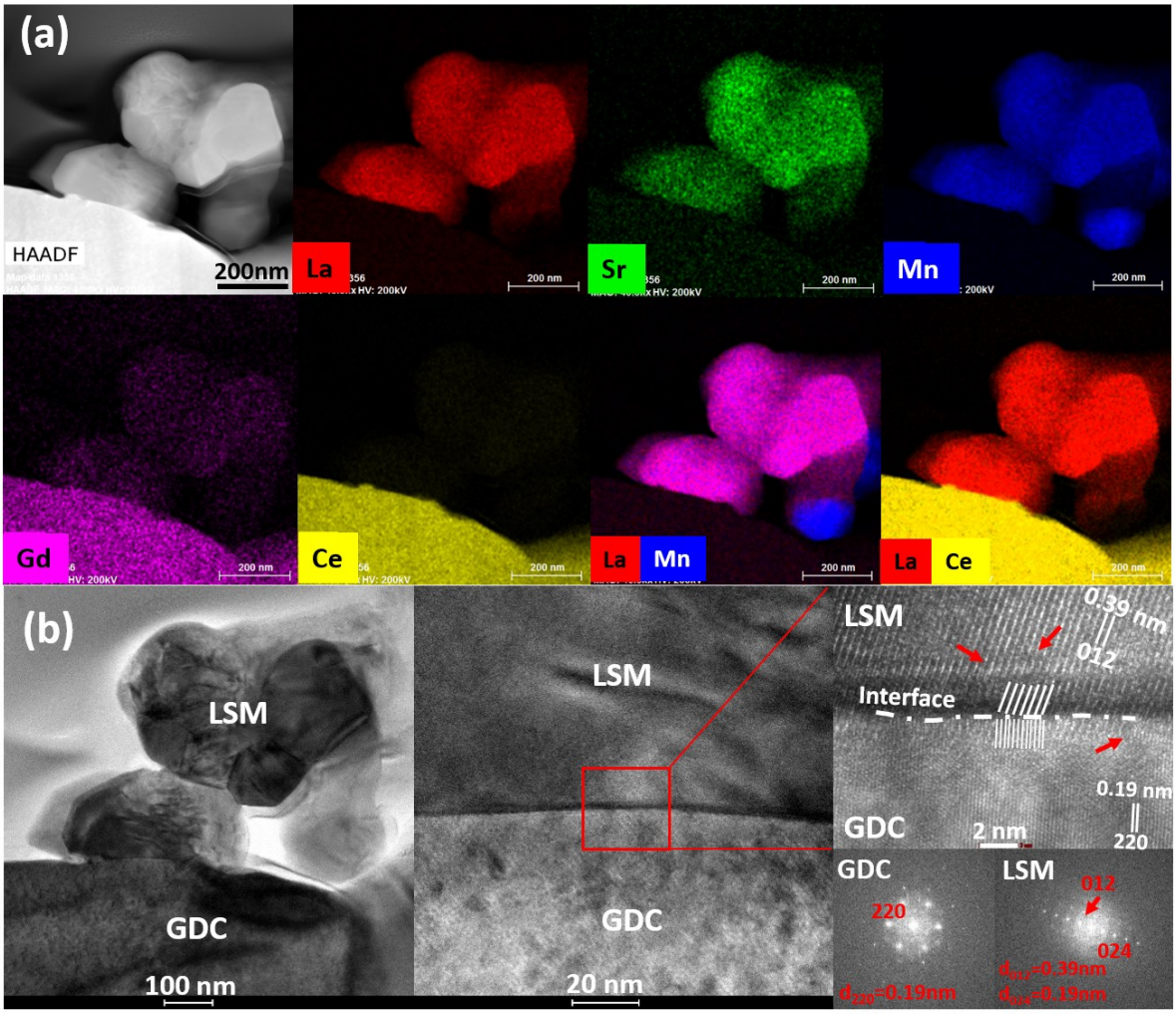

Figure 9. (a) STEM-EDS element mapping and (b) HRTEM micrographs of directly assembled LSM cathode on GDC electrolyte after polarization at 900°C and 500 $mAcm^{-2}$ for 12 h. The red arrows indicate the locations of lattice distortion.

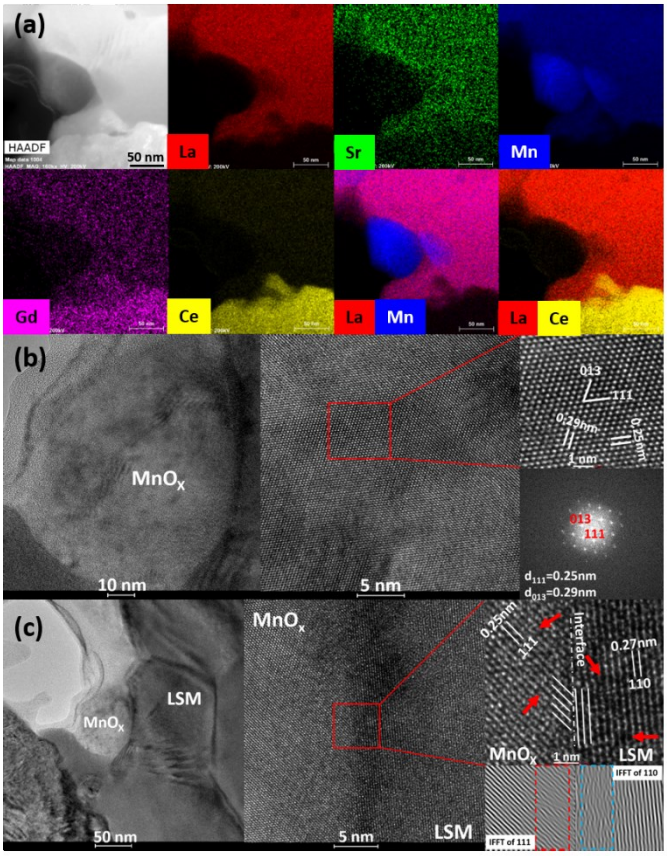

Figure 10. (a) STEM-EDS element mapping and HRTEM micrographs of (b) segregated MnO_x particle and (c) MnO_x/LSM interface after polarization at 900°C and 500 $mAcm^{-2}$ for 12 h on LSM/GDC electrode. The red arrows indicate the locations of lattice distortion.

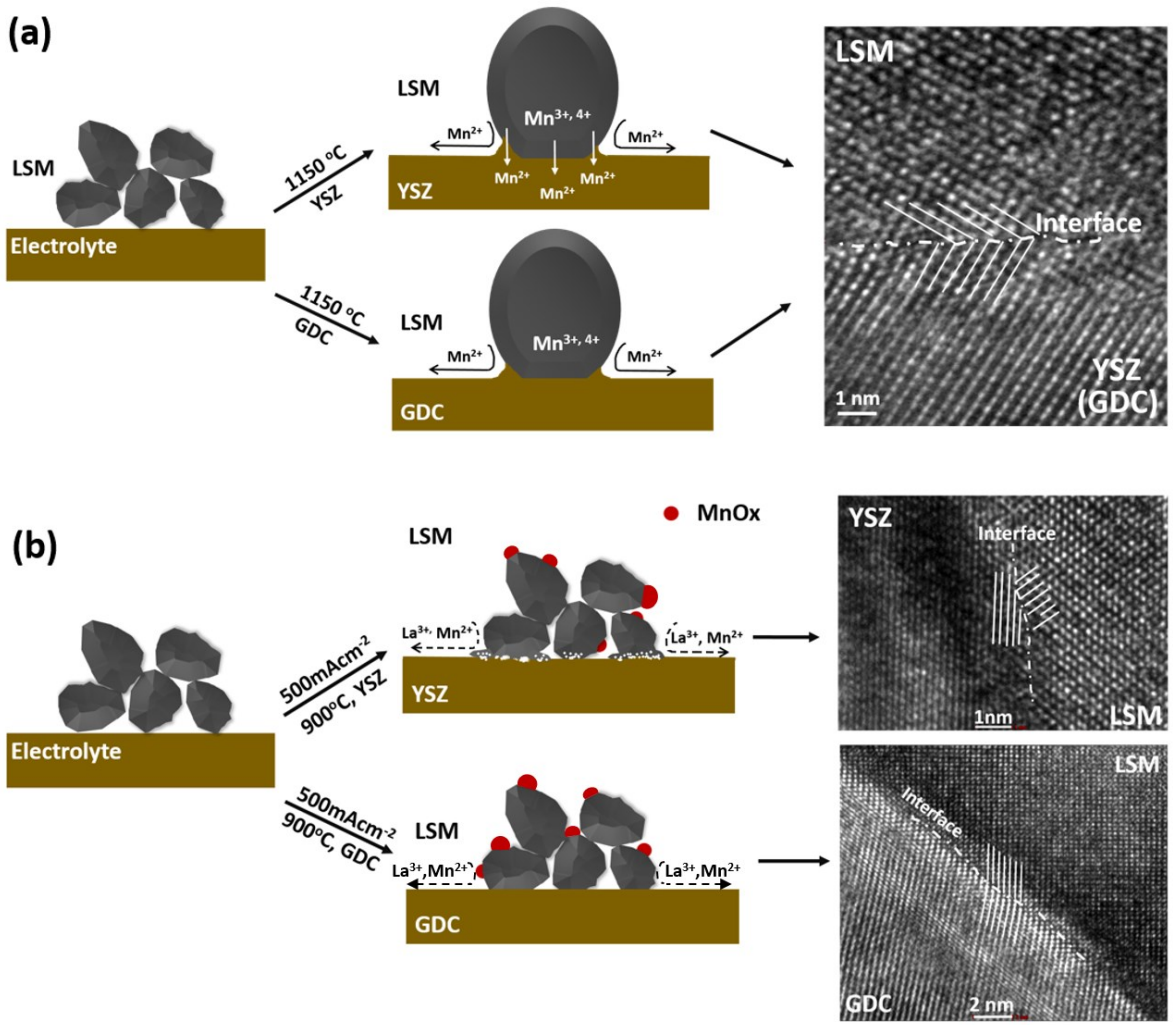

Figure 11. Schematic diagram showing the Mn diffusion and interface formation of (a) pre-sintered and (b) directly assembled LSM/YSZ and LSM/GDC electrodes.